Supplementary Information

Life history and ancestry of the Late Upper Palaeolithic infant from Grotta delle Mura, Italy

List of contents

Supplementary Figures

Supplementary Figure 1

Composite micrographs of the ULdi1 (a) and URM1 (b) portraying the tracks of the spatially resolved geochemical analyses performed by LA-(MC-)ICPMS (the narrower line is relative to the elemental analysis; the wider line, which along the EDJ covers a previous narrower line, is relative to the isotopic analysis).

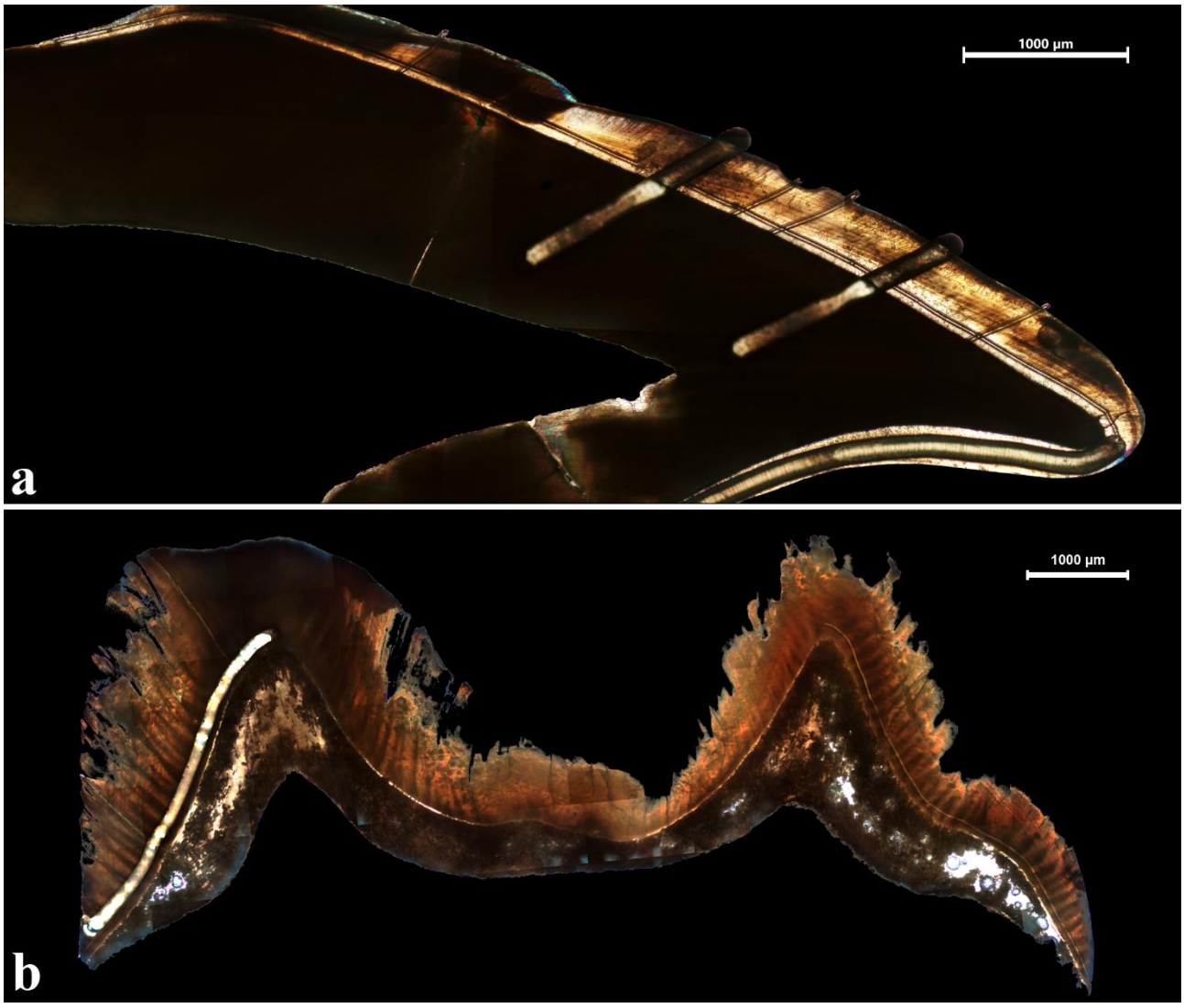

Supplementary Figure 2

Boxplot of U (left) and Mn (right) concentrations (ppm) along the EDJ path of ULdi1 (Upper Left first deciduous incisor) and URM1 (Upper Right first permanent molar). Thick line=median, box limits denote the 2nd and 3rd quartile, whiskers= minimum and maximum values. ULdi1 U: n=602, Mn: n=306; URM1 U: n=582, Mn: n=582. Source Data are found in Supplementary Data 4.

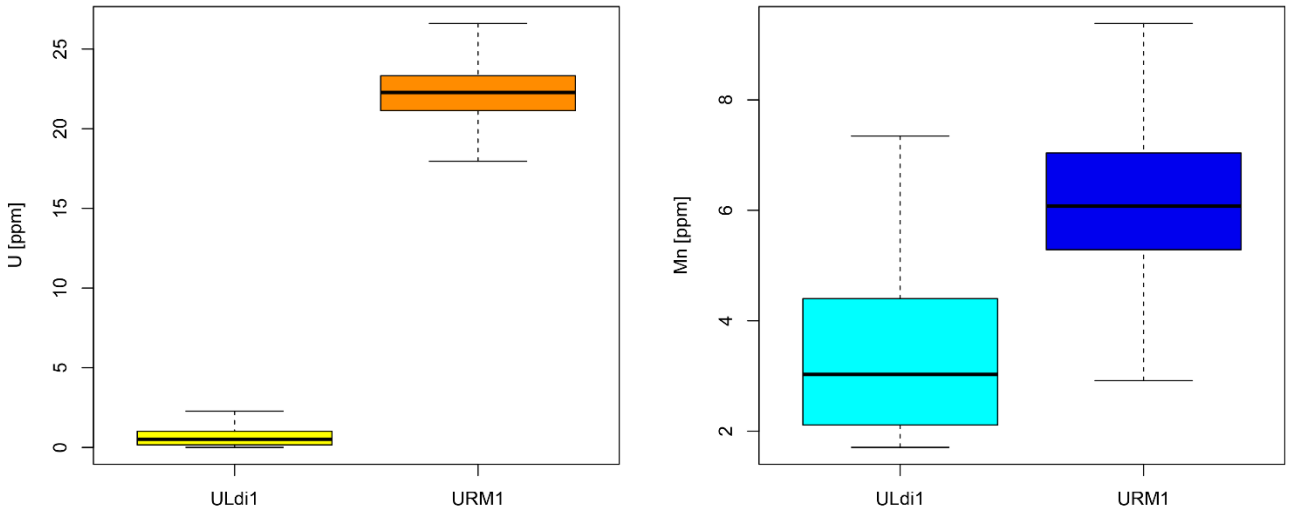

Supplementary Figure 3

Sr/Ca (top) and Ba/Ca (bottom) ratios compared with U and Mn profiles along the EDJ path of ULdi1 (darker red/blue) and URM1 (lighter red/blue). X-axis represents days of life, with 0 representing birth. Interpolation was made with a LOESS function (thick line), thin lines are 2 SE of the interpolation. Source Data are found in Supplementary Data 4.

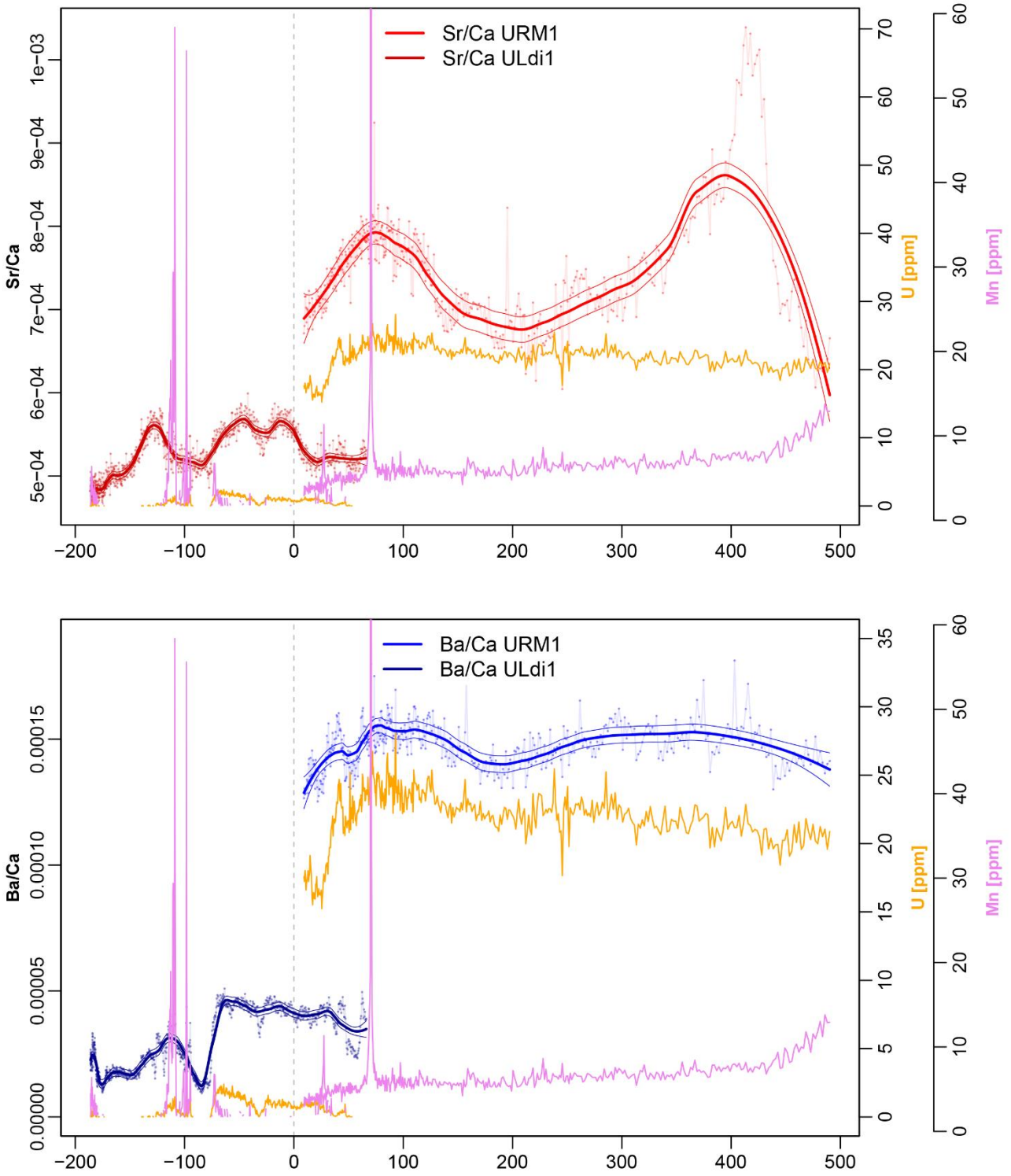

Supplementary Figure 4

Top: $^{87}Sr/^{86}Sr$ ratio (red) compared with U profile (yellow) along the EDJ path of ULdi1; X-axis represents distance along the EDJ, with 0 representing the beginning of the track. Interpolation was made with a LOESS function (thick line), thin lines are 2 SE of the interpolation. Source Data are found in Supplementary Data 5. Bottom Left: Local Sr isoscape based on the Universal Kriging model of Lugli et al (2022); the coastline is at -115 m. Bottom Right: Sr isotope value of the individual (mean ± SD of the profile in the top panel) compared with the local values extracted from the isoscape at different radii around the site.

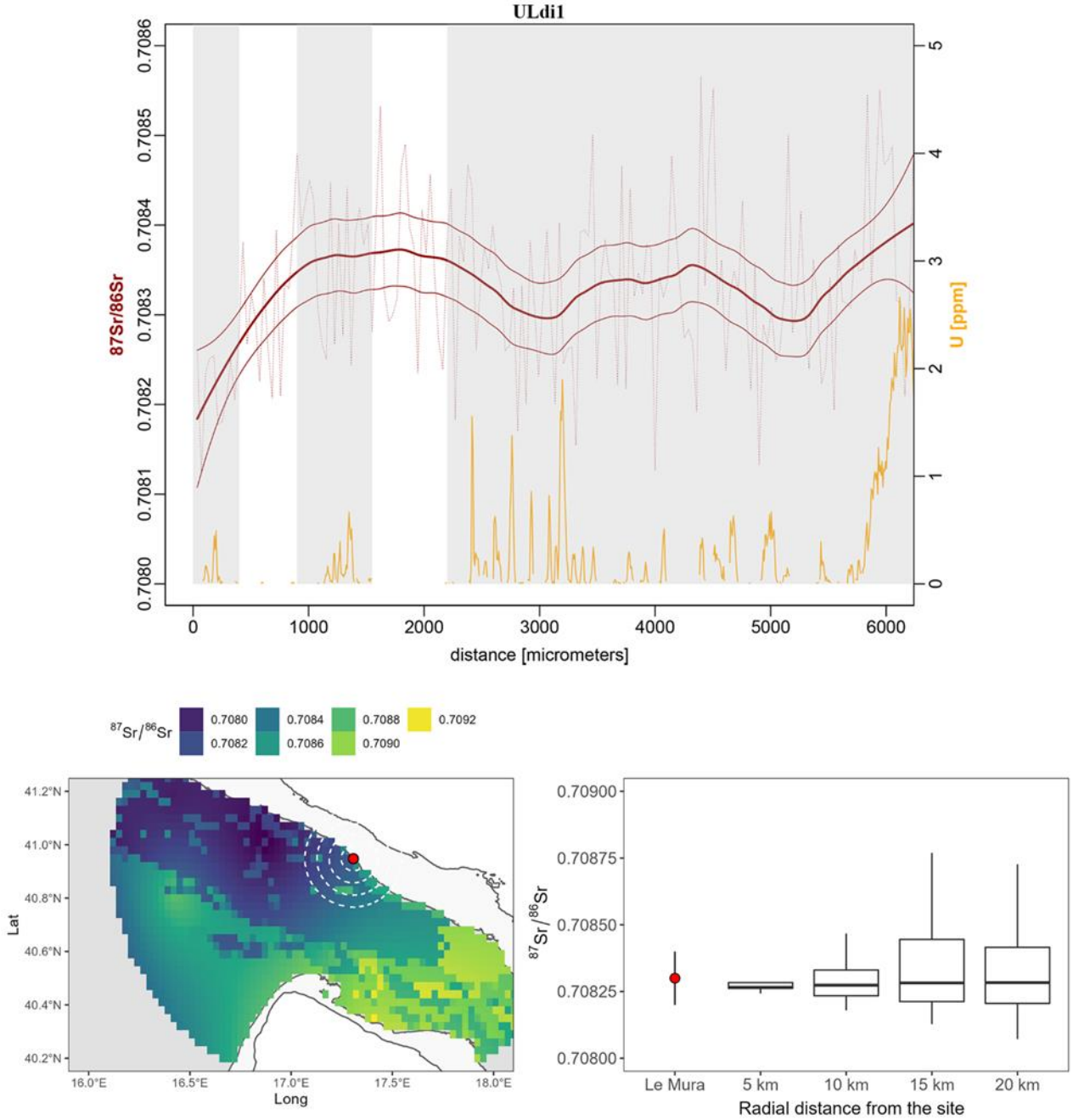

Supplementary Figure 5

Misincorporation (left) and fragmentation plot (right). The bottom plots of the misincorporation graphs, are the positions' specific substitutions from the 5’ (left) and the 3’ (right) end (red is C to T; Blue is G to A). a) Mitochondrial genome; b) Nuclear genome. Source data are provided as a Source Data file.

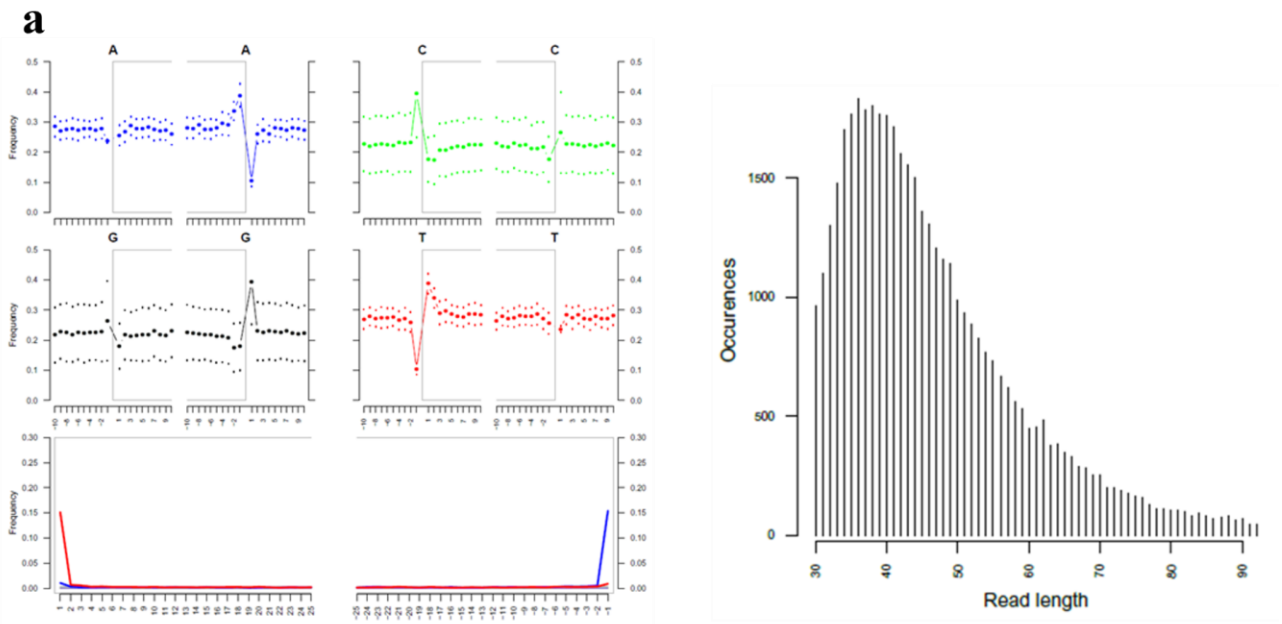

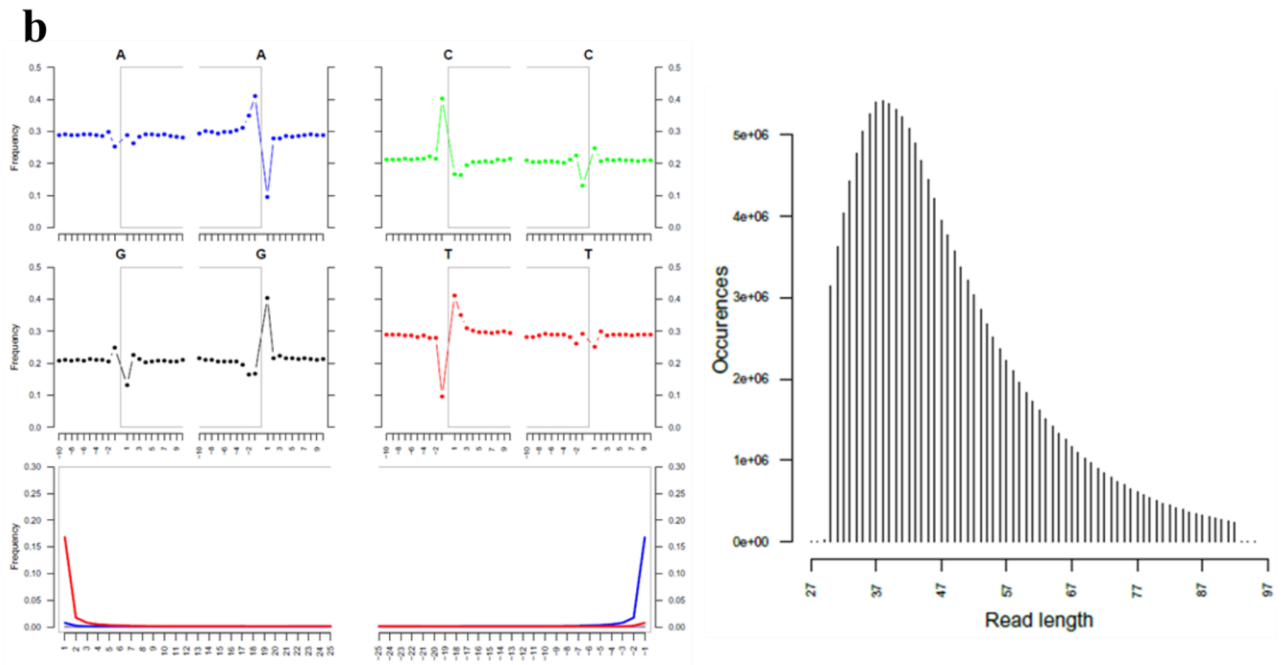

Supplementary Figure 6

a) Principal Component Analysis (PCA) of LGM and post-LGM hunter-gatherers. Ancient genomes (colored symbols) are projected on the PCA variation defined through the present-day individuals (gray dots) genotyped on the Human Origins dataset. Representative ancient genomes (reported in Supplementary Data 12) are shown in outlined dots colored based on their genetic cluster, as illustrated in the legend on the right of the PCA. The newly reported individual (Le Mura 1) is shown in black-outlined and filled diamond; b) Multi-Dimensional Scaling (MDS) plot of European hunter-gatherers based on $1 - f3$(Le Mura 1, *X*; Mbuti.SDG related to Figure 4. Samples dated to the Pre-LGM are coloured in blue, Post-LGM in green, Late Glacial in magenta and Holocene hunter-gatherers in red. Source data are provided as a Source Data.

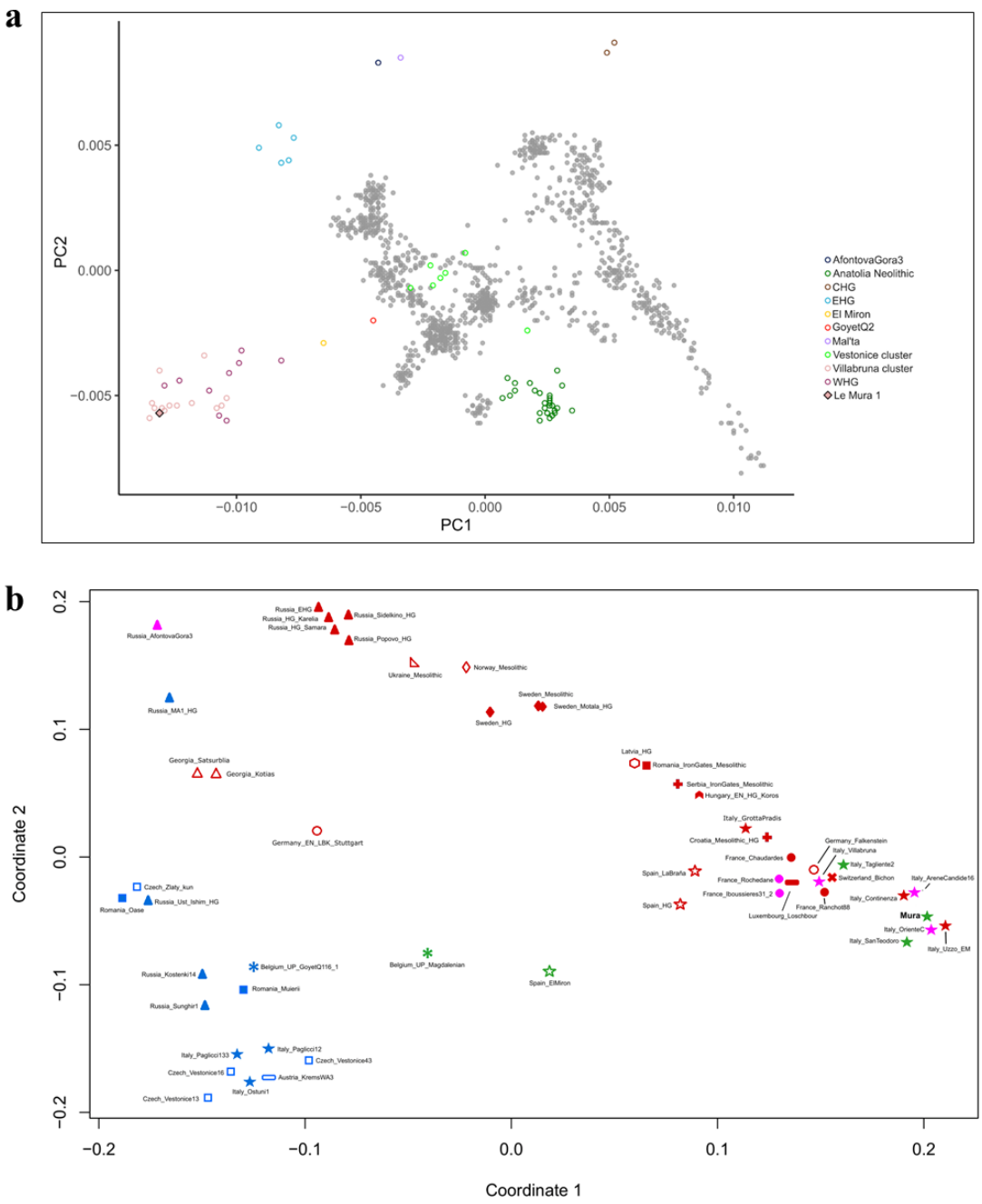

file.

Supplementary Figure 7

Shared genetic drift between Le Mura 1 and other ancient samples from an outgroup (in this case the African population Mbuti) estimated through outgroup *f3*-statistic in the form *f3*(Le Mura 1, *X*; Mbuti), where *X* are samples listed in the x-axis. Bars represent the standard error deviation from the statistic value. Samples dated to the Pre-LGM are coloured in blue, Post-LGM in green, Late Glacial in magenta and Holocene hunter-gatherers in red. Source data are provided as a Source Data file.

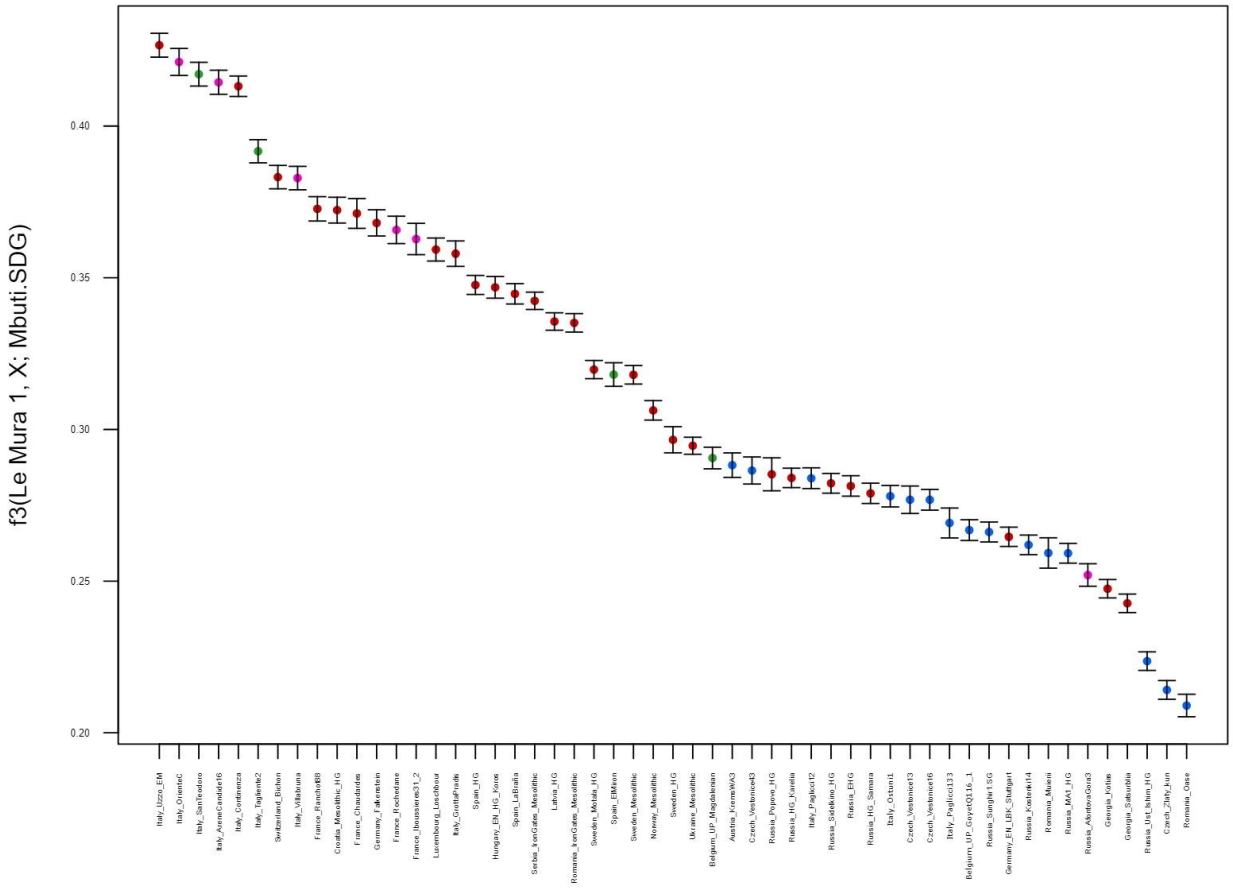

Supplementary Figure 8

Pairwise mismatch rates (PMR) between Italian Epigravettians and Mesolithic individuals of different groups. a) Le Mura 1 is included in Group 2. b) Le Mura 1 is included in Group 3. Data values and dispersion increase more when Le Mura 1 is included in Group 3, rather than in Group 2, suggesting that the population of continental southern Italy had a genetic variability which was higher than the Sicilian group and more comparable to the population of Central Italy. Samples included in each group are reported in Supplementary Data 18. In the box plot the centre line is the median, box bounds delineate the interquartile range and whiskers extend to maximum and minimum values. Source data are provided as a Source Data file.

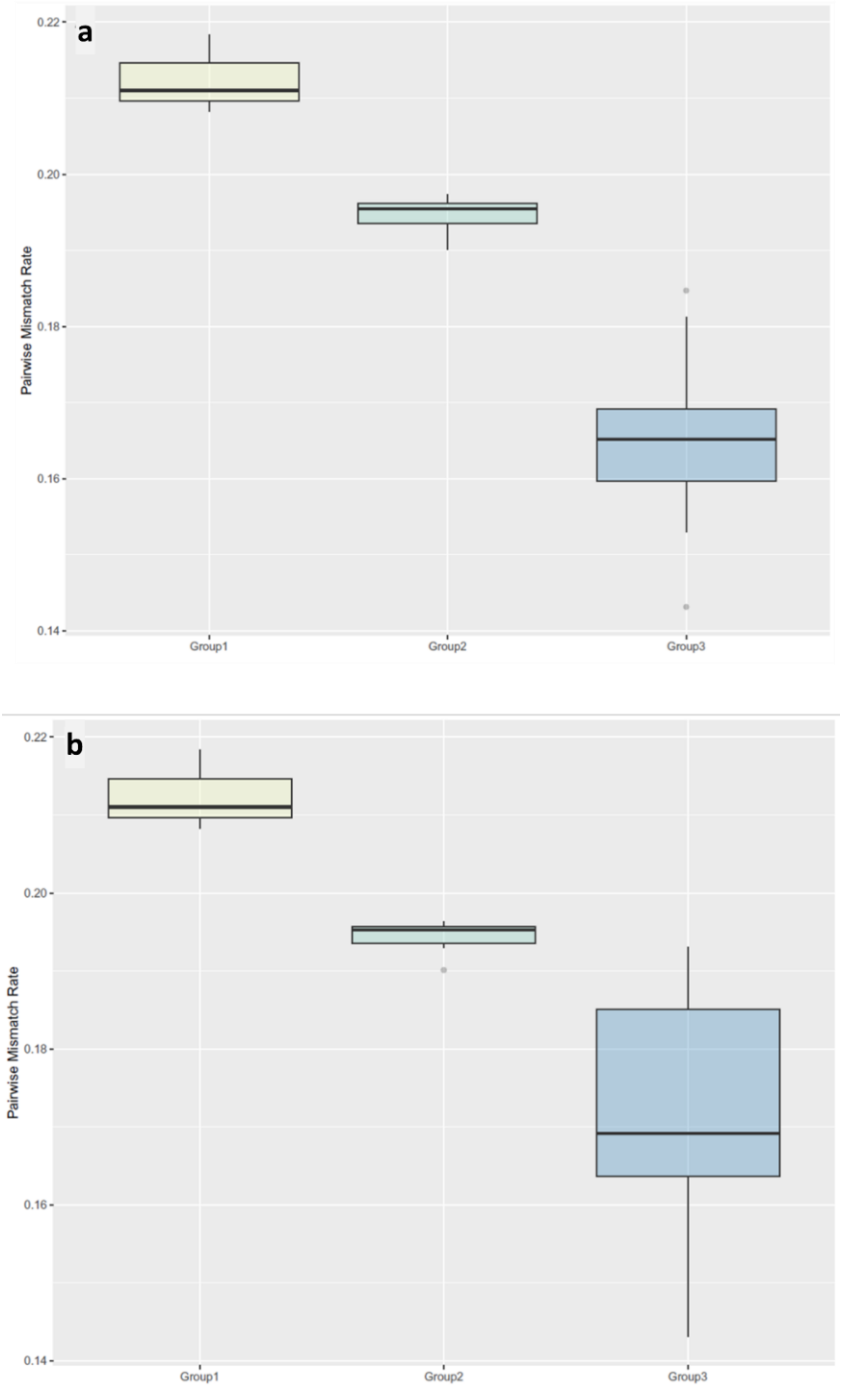

Supplementary Figure 9

D statistics to estimate admixture with archaic humans, a) Neanderthal Vindija 33.19 or b) Denisova 3 genome. Y axis shows the amount of D statistics; the standard error was calculated by Jackknife method using 555 blocks and it is denoted by bars. Source data are provided as a Source Data file.

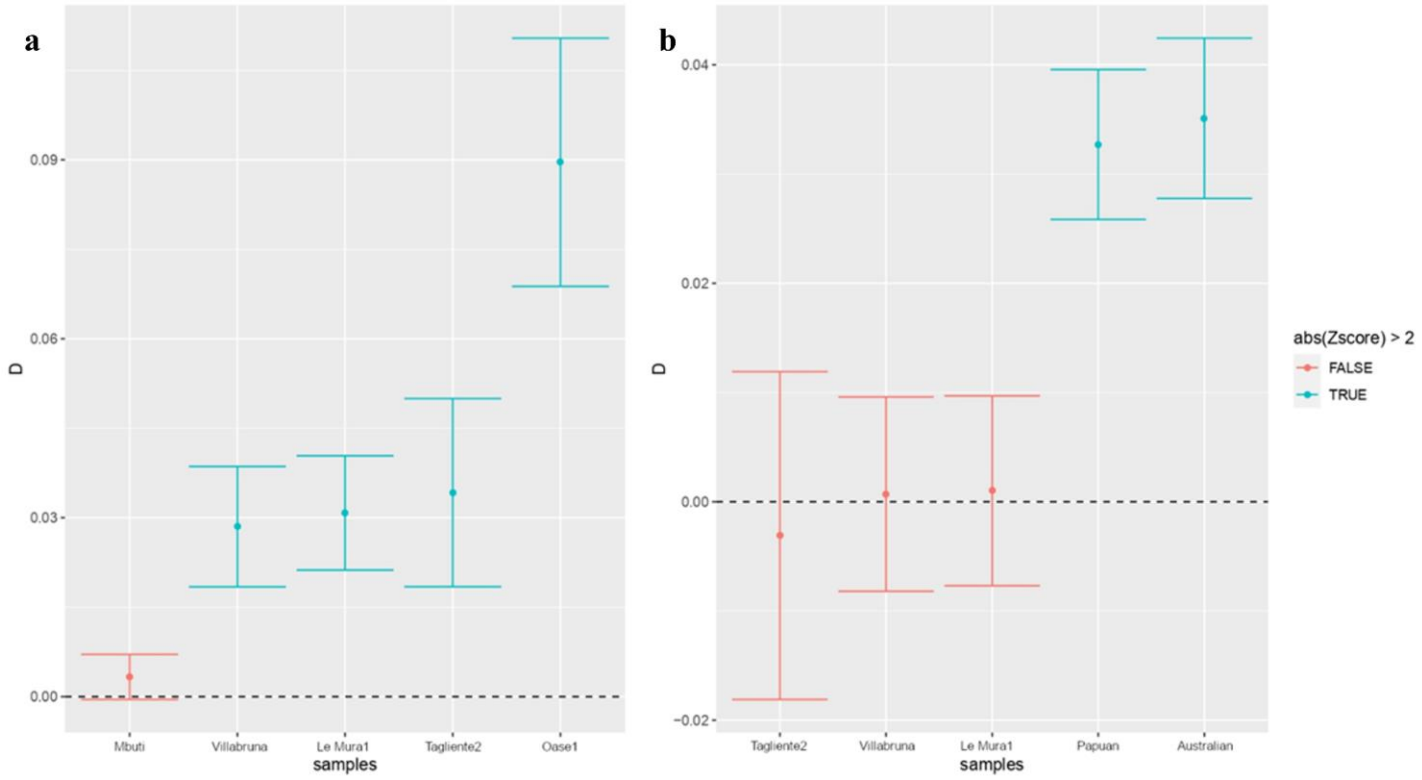

Supplementary Figure 10

Estimation of the proportion of archaic ancestry using *f4* ratio statistics. (a) Neanderthal ancestry estimation. (b) Denisova ancestry estimation. Y axis shows the amount of *f4* ratio; the standard error was calculated by Jackknife method using 555 blocks and it is denoted by bars. Source data are provided as a Source Data file.

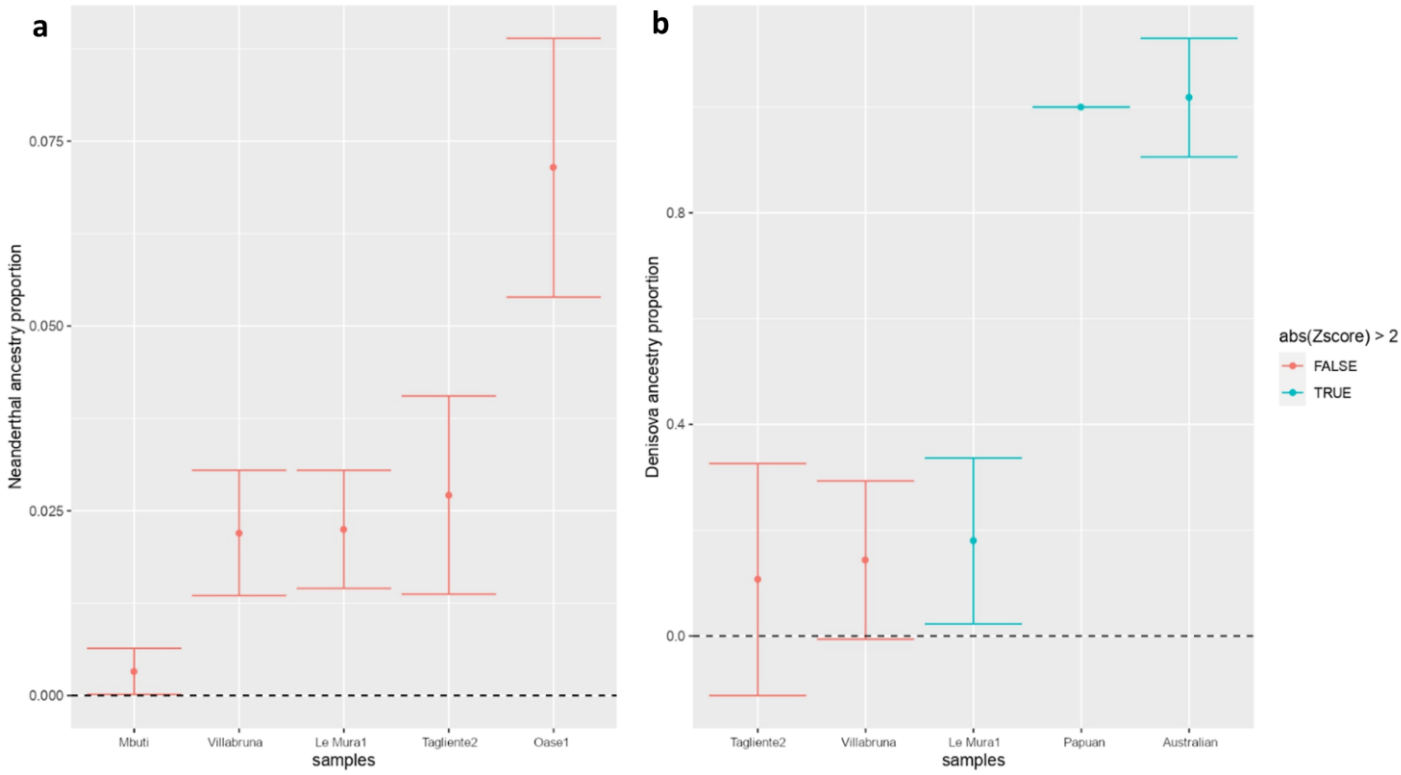

Supplementary Figure 11

Neanderthal and Denisova fragments distribution along the genome of Le Mura 1.

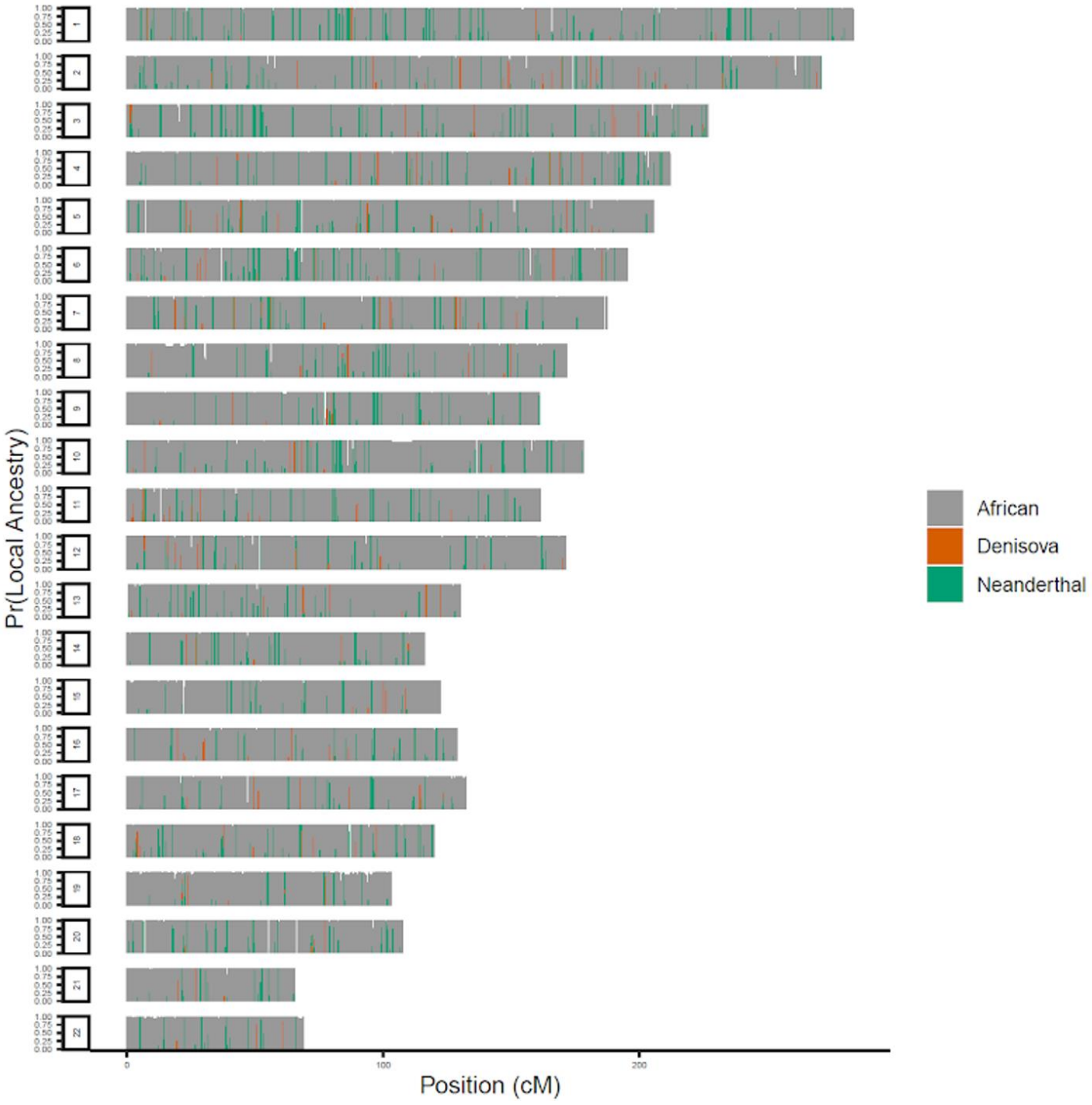

Supplementary Figure 12

Maximum Parimony tree of 53 Present-Day and 77 Pre-Neolithic mitogenomes. Samples dated to the Pre-LGM are coloured in blue, Post-LGM in green, Late Glacial in magenta and Holocene hunter-gatherers in red.

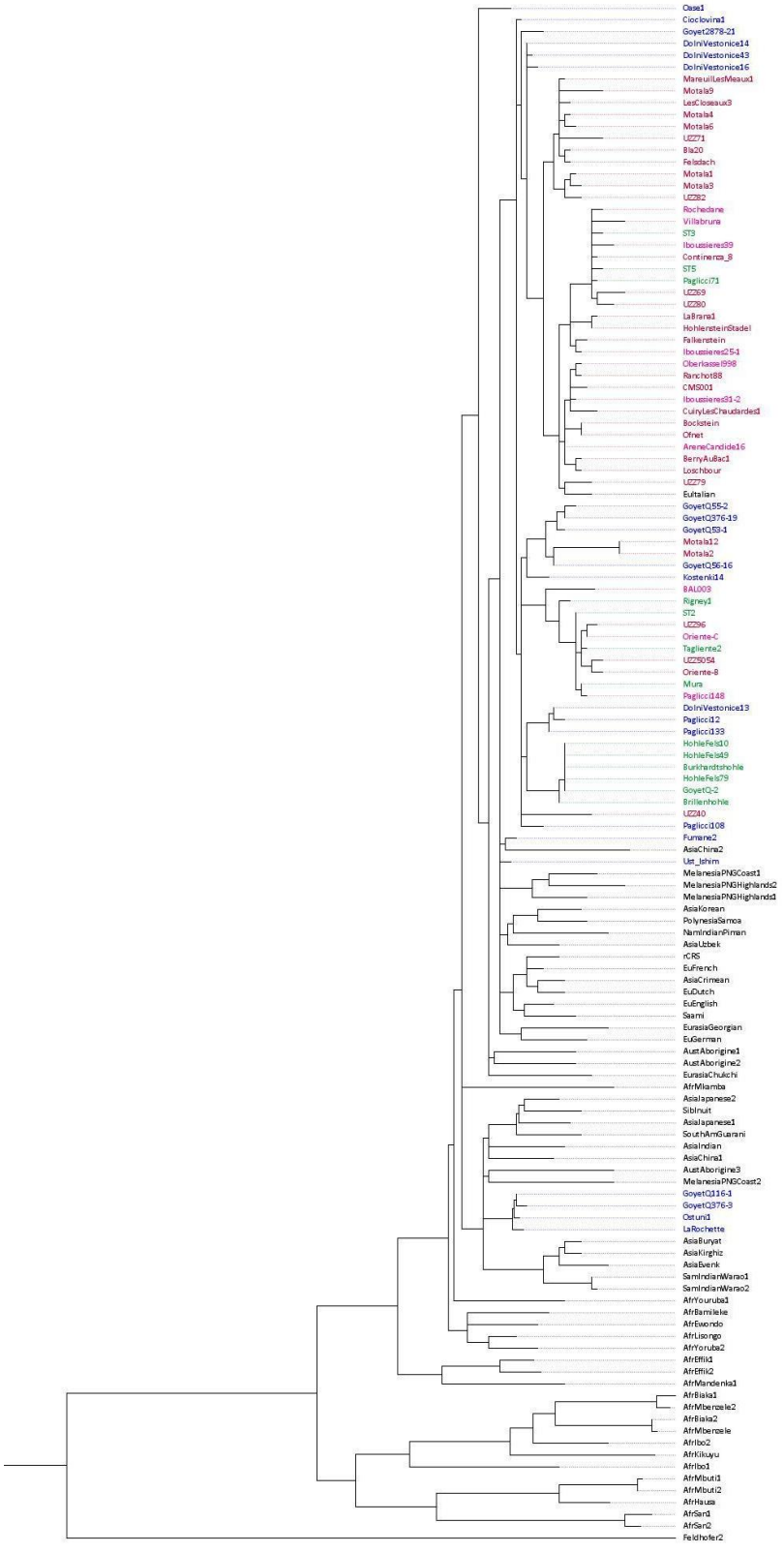

Supplementary Figure 13

Schematics of the protocol for the creation of digital models of missing/sampled portions by using reverse engineering techniques.

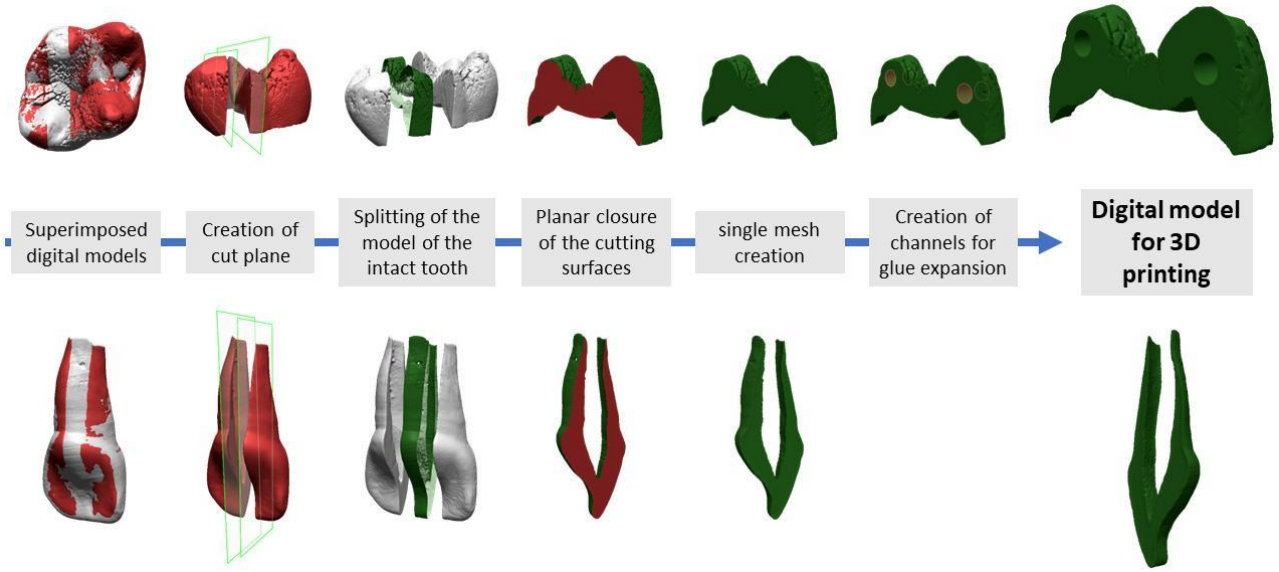

Supplementary Figure 14

Photographic record of the URM1 in occlusal view after physical restoration. Scale bar is 5 mm.

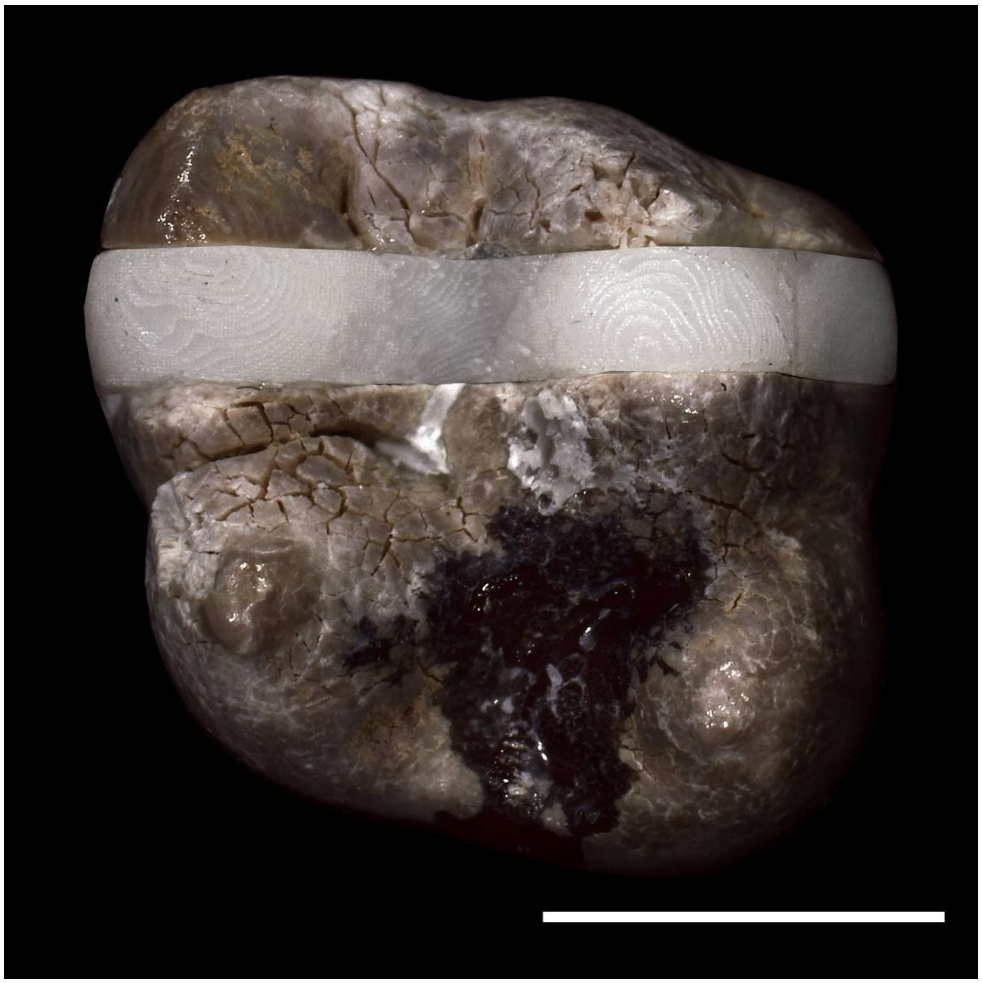

Supplementary Figure 15

Photographic record of the ULdi1 in buccal (B) and lingual (L) views after physical restoration. Scale bar is 5 mm.

Supplementary Notes

Supplementary Note 1: Archaeological context

Grotta delle Mura is a karstic cavity located along the coast, at the bottom of a small bay in the southern outskirts of the town of Monopoli (BA, southern Italy) (Supplementary Figure 16). After a first phase of investigation (F. Anelli 1953-57, O. Cornaggia Castiglioni 1961-63 and 1966) [1] and a long period of abandonment, research was resumed in 1985 by the Dipartimento di Archeologia e Storia delle Arti of the University of Siena, under the direction of one of the writers (M. C.). The excavations covered two contiguous areas (A and B), covering approximately 21 m^2. The grave of the infant was discovered in 1998 in the second of these areas, where the stratigraphic sequence (Fig. 1b) was better preserved. For logistical and preservation reasons, the cranium had to be excavated the first year, whereas the rest of the remains were excavated the following excavation campaign.

Supplementary Figure 16. View of the cave's entrance as seen from the coast (Photo by Mauro Calattini).

The complete cultural sequence (Fig. 1b), integrated between the two areas, starts at the bottom with a Mousterian level (typical Mousterian 44530 ± 2040 BP; 54840-44392 cal BP 95.4%) (Beta 142777) [2], which is followed, after a considerable time hiatus, by a series of levels referable to the Epigravettian cycle, partly still unpublished. The latter include levels of the Early Epigravettian cran subphase (15860 ± 80 BP; 19392-18933 cal BP 95.4%) (Beta 171353) [3], a layer probably referable to the Evolved Epigravettian and, following this, the Final Epigravettian layer (SU 130), within which the burial in question was discovered. The sequence is completed by a Mesolithic layer (Sauveterrian) (8290 ± 50 BP; 9451-9038 cal BP 95.4%) (8240 ± 120 BP;

9527-8811 cal BP 95.4%) (Utc. 1417 and 780) [3] and finally, based on the pottery, a layer referable to the final Early Neolithic in Apulia. The dates reported above are calibrated with the IntCal20 curve in the OxCal 4.4 software [4,5].

The remains of the infant were found leaning against a large collapse rock, partly jutting out over them (Supplementary Figure 17). The skeletal remains were covered by two flat stones placed at right angles to each other (Supplementary Figure 18a), one at foot level and the other covering the body, like a sheet, up to the jaw. Only the head was left uncovered, which in turn was slightly wedged between two smaller stones (Supplementary Figure 18b). Given the sandy soil, there is no certainty whether the body had been laid in an intentional pit [6]. The body lay supine with its arms along the sides, and a north-west/south-east (head/feet) orientation (Fig. 1c; Supplementary Figure 18c). The remains are well preserved and mostly intact. No red ochre, nor grave goods were present, though it was attributed to the Final Epigravettian based on stratigraphic association.

Supplementary Figure 17. Picture of the discovery of the cranium below the jutting out collapse rock (Photo by Mauro Calattini).

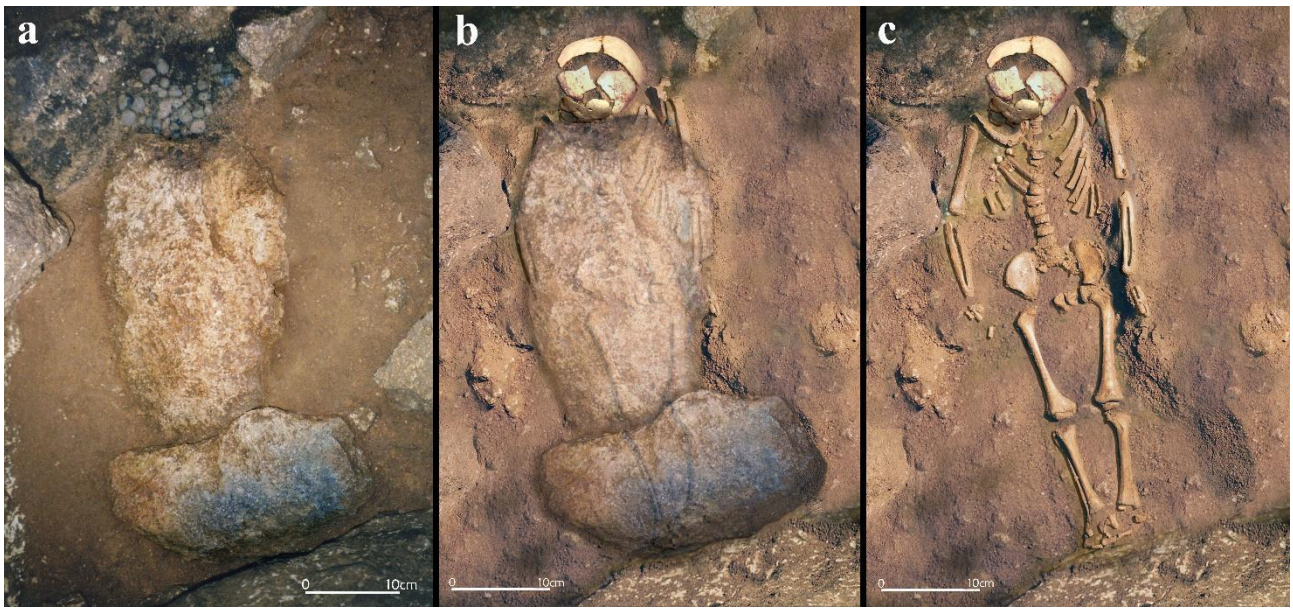

Supplementary Figure 18. a) Zenital picture of the blocks still in the deposit; b) Representation of the position of the blocks relative to the skeletal remains (along with the superimposition of the blocks, the cranium was also digitally added-in to show its original position); c) Picture of the disposition of the skeletal remains (the cranium was digitally added-in to show its original position) (Photos by Mauro Calattini; The old excavation slides were processed and re-elaborated by Stefano Ricci).

With regard to environmental data, there are currently preliminary observations on the macrofauna and preliminary sedimentological analyses [7]. Among the faunal remains, although there is a predominance of aurochs (*Bos primigenius*) and the presence of wild boar (*Sus scrofa*), in this layer there is the highest percentage of equidae (*Equus ferus* and *Equus hydruntinus*) found so far in the entire sequence, which is associated with a strong presence of lagomorphs. Such an association suggests the presence of a cold climate arboreal grassland. The environment outlined above (with wide open spaces) would perfectly explain the aeolian transport of the sandy sediments which form the burial's level. Although preliminary, the palaeoenvironmental data are confirmed by what is known for the same region (Apulia) at similar chronologies [8]. In the area of Grotta delle Mura, the persistence of this arid condition will provide an important refuge area for equids during the Early Holocene [9].

From a cultural point of view, SU 130 was traced back to an early phase of the Italic Final Epigravettian, before the appearance of the Romanellization phenomenon, which is a facies that affected the last phases of the Salentine Final Epigravettian. The presence of numerous carbonaceous frustules allowed the radiometric dating, with no ultrafiltration, of the level containing the burial to 11420 ± 100 BP (13480-13118 cal BP 95.4%) (Beta 142778) [2].

Supplementary Note 2: Anthropological Study

The physical anthropological analysis of Le Mura 1 was carried out within the frame of a degree thesis in 2019. The majority of the skeletal elements remain intact, rendering the skeleton largely complete; the absence of certain elements or portions of bone is attributed both to conservation issues and to the fact that they may not have yet developed at the time of death. Due to the immature status of the individual, with secondary sexual characteristics not yet manifest, sex determination based on skeletal analysis was not feasible. An estimated stature of approximately 80 cm was derived using the length of the femoral diaphysis (Supplementary Table 1), following [10]. Age at death was estimated by means of two main methods: analysis of tooth root and crown

development, and analysis of skeletal development. For dental analysis, the developmental stages of root and crown proposed by [11,12] and utilised in the study by [13] was applied. This analysis was facilitated by the exceptional state of preservation of the teeth, and was performed on the loose teeth that could be removed from their sockets. For each of these teeth, the stage of tooth formation (hereinafter referred to as 'stage') and the estimated age at death range are reported [11–13]. It is pertinent to note that the ages expressed in months denote the midpoint within a three-month span, whereas ages articulated in years signify the midpoint within a one-year interval, as reported by [13]:

- URdm2 - stage: "Crc", age: 7.5 months – 1.5 years;
- ULdm2 - stage: "Crc", age: 7.5 months – 1.5 years;
- LLdm1 - stage: "R ½", age: 10.5 months - 1.5 years;
- LRdm1 - stage: "R ½", age: 10.5 months - 1.5 years;
- LLdi1 - stage: "R ¾", age: 10.5 months - 1.5 years;
- LRdi1 - stage: "R ¾", age: 10.5 months - 1.5 years;
- URdi1 - stage: "R ¾", age: about 1.5 years;
- ULdi1 - stage: "R ¾", age: about 1.5 years;
- LLdi2 - stage: "R ½", age: about 10.5 months;
- LRdi2 - stage: "R ½", age: about 10.5 months;
- ULdi2 - stage: "R ¾", age: 10.5 months - 1.5 years;
- URdi2 - stage: "R ¾", age: 10.5 months - 1.5 years;
- URdc - stage: "R ¼", age: about 1.5 years;
- ULdc - stage: "R ¼", age: about 1.5 years;
- URM1 - stage: "Cr ½", age: 1.5 years - 3.5 years.

In the analysis of skeletal development, factors such as the fusion of vertebral arches, both anteriorly and posteriorly, the emergence of certain ossification centres, especially within the carpal bones, and osteometric measurements were considered. A digital caliper was used for the measurement of the maximum length of long bones, subsequent to which the linear regression equations developed by [14] and reported in [15] were applied (Supplementary Table 1). The comparative analysis of the methodologies used for both dental and skeletal development, indicate an age at death ranging between 7.5 months and 1.5 years. For additional comparison and to ensure the comprehensiveness of the data, an analysis on the degree of tooth wear of the above-mentioned teeth was also carried out, following [16] and [17]. As expected, minimal wear was observed for each tooth, estimated as "N" [16] and "1" [17]. In the context of the individual's health status, the palaeopathological analysis conducted at the dental level did not reveal the presence of any notable oral pathologies or the occurrence of enamel linear hypoplasia (with the exception of ULdi1, see main text). At the skeletal level, a probable 'greenstick' fracture of the left clavicle was identified: examination of the acromioclavicular portion revealed the presence of a bony callus, contributing to an abnormal morphology of this anatomical region (Supplementary Figure 19). Among possible causes, one hypothesis is a birth complication known as 'shoulder dystocia', which might result in a fracture of the clavicle. This complication occurs when the foetus, in cephalic position, fails to disengage the shoulders during the contraction following head disengagement, contrary to the typical birthing process, or it may result from an improper manoeuvre by the operator [18]. Consequently, this leads to the foetus' body being retained against the mother's pelvis [19].

Supplementary Figure 19

Left (L) and Right (R) clavicles; u: upper view; i: inferior view

Supplementary Table 1

Maximal length of long bones and estimated age at death

Element	**Maximal length (cm)**	**Age at death (years)**
Humerus	10.4	1 – 1.5
Radius	8.2	1 – 1.5
Ulna	9.2	1 – 1.5
Femur	13	1 – 1.5
Tibia	10.7	1 – 1.5
Fibula	10.5	1

Supplementary Note 3: Description of ULdi[1] and URM[1] dental specimens

ULdi[1]

This specimen is an upper left central deciduous incisor (ULdi[1]). The crown has no occlusal wear (stage 0 based on [17]). From the labial view, the crown has moderate labial convexity (ASUDAS grade 3), which becomes less pronounced distally. The lingual surface is concave, and exhibits a distal and mesial marginal ridge as well as a median ridge, which disappears as it reaches the cervical eminence (Supplementary Figure 20). The root's developmental stage is R ¾ (with a developed portion of 7.96 mm). The tooth crown has a MD diameter of 6.8 mm and a BL diameter of 5.6 mm. At the cervix, the MD diameter is 5 mm and BL diameter is 4.29 mm. Linear and volumetric measurements of dental tissues are reported in Supplementary Table 2.

Supplementary Figure 20

A) Digital model of the Upper Left di1 in different views. B) The enamel-dentine junction of the tooth shows some ridges on the lingual area. Abbreviations: O = occlusal; B = buccal; L = lingual; D = distal; M = mesial. Scale bar = 1 cm.

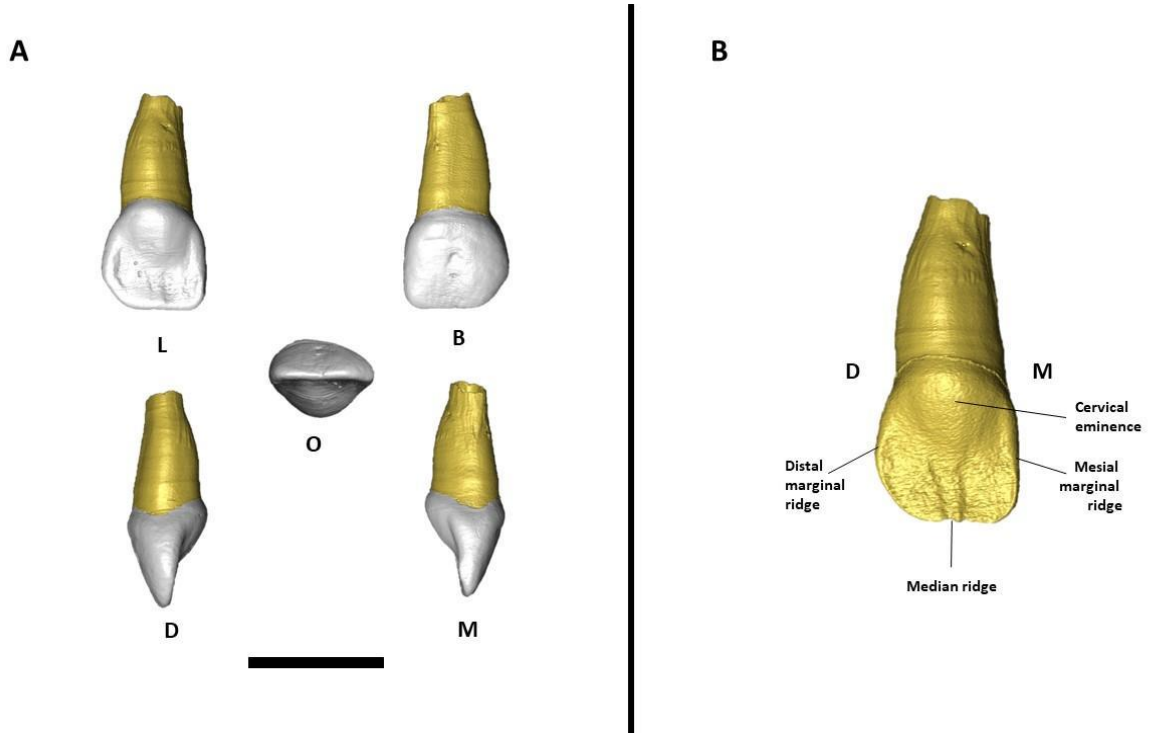

Topographic maps of the enamel thickness show thinner enamel on the distal and lingual side than on the mesial and buccal, where the range of colours shows extreme thickness values in particular on the mesial ridge (Supplementary Figure 21).

Supplementary Figure 21

3D enamel thickness distribution maps of the Upper Left di1 visualized using spectral colours. While the thickest enamel is represented in red, the thinnest enamel appears in violet (see colour-scale with the corresponding enamel thickness in mm). Abbreviations: O = occlusal; B = buccal; L = lingual; D = distal; M = mesial. Scale bar = 1 cm.

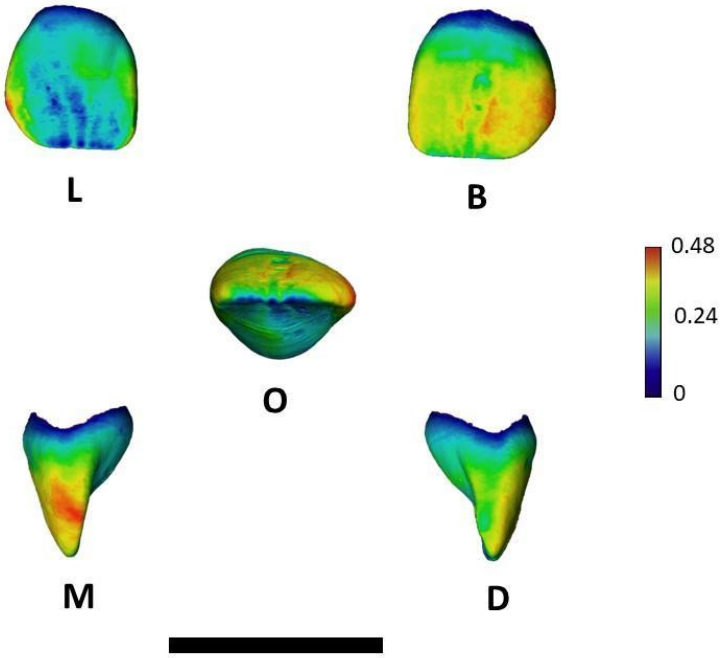

URM[1]

The tooth is an upper right first molar (URM[1]) with a completed cusp outline (Cr ½ of [12]). As the tooth was not yet erupted, the crown has no stage of occlusal wear (stage 0 based on [17]). The three main cusps of the trigone are preserved and the hypocone shows an enlargement distally. These three cusps along with grooves, crests and accessory cusps are visible on the EDJ (Supplementary Figure 22). The paracone is the larger cusp, followed by the hypocone, the protocone, and finally by the metacone. The protocone size is reduced, owing to a large Carabelli's tubercle, corresponding to grade 5 according to [12] (Fig. 3) and due to an enlargement on the mesial side. The protocone is in contact with the metacone through an oblique crest, from which secondary crests depart.

Supplementary Figure 22

A) Digital model of the Upper Right M1 in different views. B) The enamel-dentine junction of the tooth shows the Carabelli's tubercle and the oblique crest of the crown. Abbreviations: O = occlusal; B = buccal; L = lingual; D = distal; M = mesial. Scale bar = 1 cm.

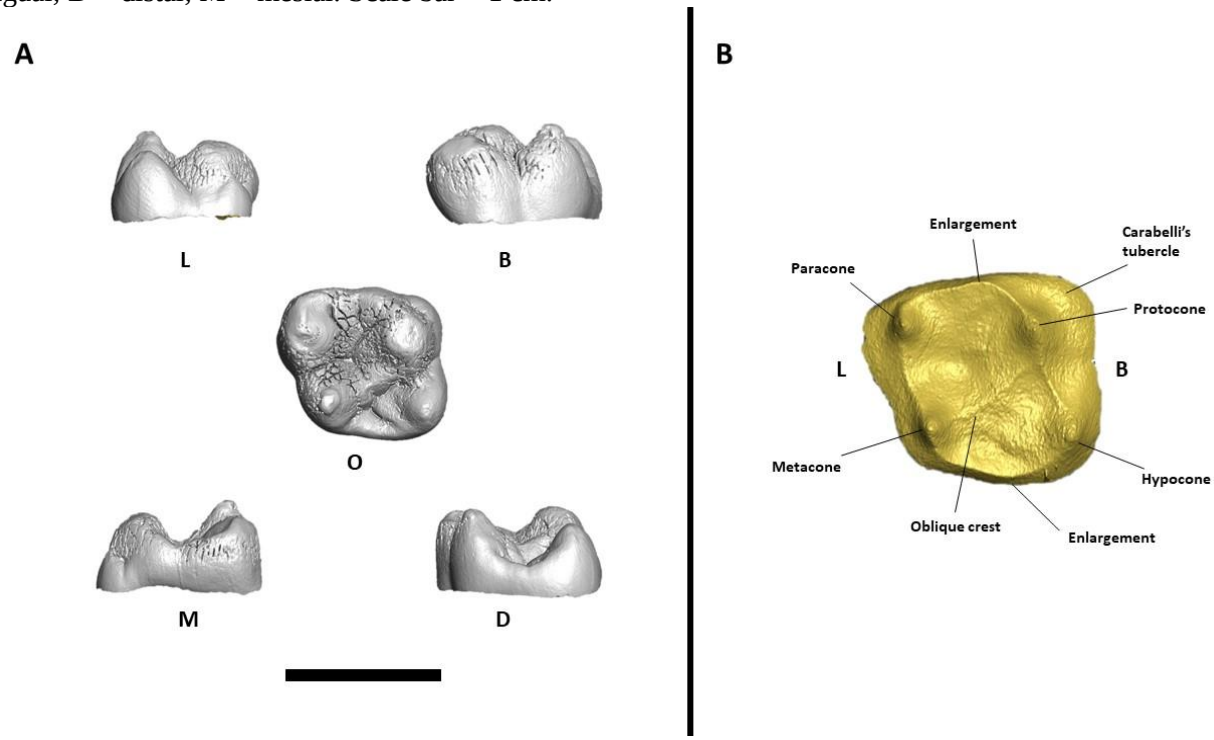

The degree of development is of Cr ½ [12]. Neither caries nor enamel hypoplasia are present. The tooth crown has a MD diameter of 9.04 mm, and a BL diameter of 10.33 mm. Volumetric measurements of dental tissues are reported in Supplementary Table 2.

Topographic maps of the enamel thickness present a very different aspect. It shows thinner enamel (intermediate thickness values colour coded as green or yellow) on the Hypocone than on the other cusps, which present a wide range of colours showing extreme thickness values (dark red), in particular on the paracone. The latter, shows enamel values thicker on the mesial and buccal side than on the lingual slope (Supplementary Figure 23).

Supplementary Figure 23

3D enamel thickness distribution maps of the Upper Right M1 visualized using spectral colours. While the thickest enamel is represented in red, the thinnest enamel appears in violet (see colour-scale with the corresponding enamel thickness in mm). Abbreviations: O = occlusal; B = buccal; L = lingual; D = distal; M = mesial. Scale bar = 1 cm.

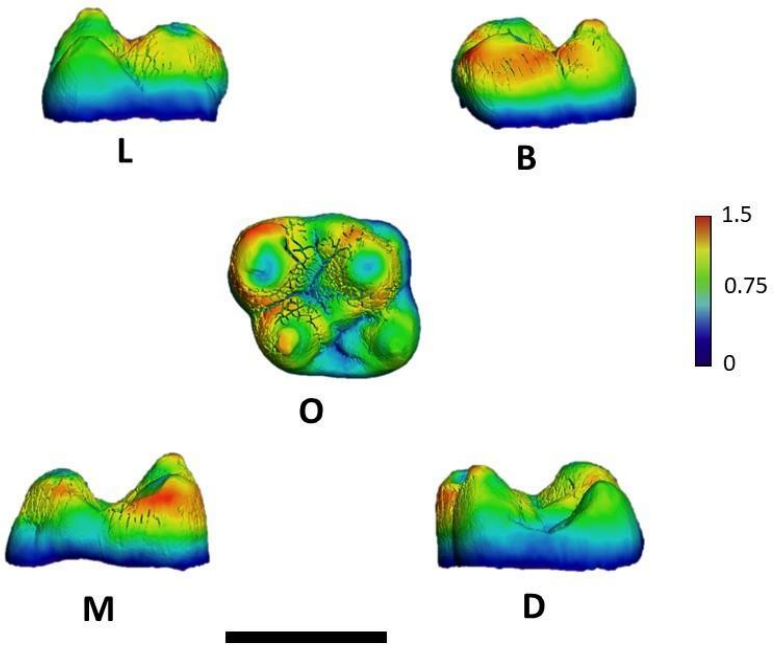

Supplementary Table 2

3D values of enamel thickness

	Enamel Volume	**Dentine Volume**	**EDJ**	**3D AET**	**3D RET**
URM[1]	118,88	92,77	118,8	1,00	22,10
ULdi[1]	25,33	67,88	88,29	0,29	7,03

Abbreviations: EDJ = enamel-dentine junction; AET = average enamel thickness; RET = relative enamel thickness.

Supplementary Discussion

Paleogenomics

Uniparental markers information. Using Haplogrep2 [20,21], Le Mura 1 was assigned to the U2'3'4'7'8'9 mitochondrial haplogroup. The earliest occurrence of U2'3'4'7'8'9 lineage in Europe has been documented in a pre-LGM individual from Grotta Paglicci in southern Italy (Paglicci 108), dated around 28,000 years BP [22]. Immediately after the LGM, this haplogroup is detected in a specimen coeval to Le Mura 1 from northern Italy (Tagliente 2) [23] and in southern Italy and Sicily, where U'2'3'4'7'8'9 is the most frequent lineage among Late Pleistocene and Holocene individuals [24–27]. In the phylogenetic tree (Supplementary Figure 12 and Supplementary Data 26), the sequence of Le Mura 1 falls within the Italian clade of U2'3'4'7'8'9, which branches from the ancestral node – dated to 25,430 years BP (95% HPD: 20,732-30,880) – after the separation of Rigney 1, an individual in France which was assigned to the same haplogroup [22]. In Europe, another sample belonging to the U2'3'4'7'8'9 lineage is an individual from Balma Guilanyà in the Iberian Peninsula dated to 12,000 years BP [28], which falls in a separate branch of the post-LGM cluster (Supplementary Figure 12), with an estimated divergence time of 32,211 (95% HPD: 25,944-38,561) (Supplementary Data 28). The time to the most recent common ancestor (TMRCA) for the U2'3'4'7'8'9 clade was estimated at 42,622 years BP (95% HPD: 36,625-48501) (Supplementary Data 28), in agreement with independent estimates from modern mitogenomes [29]. Other divergence times for the U2'3'4'7'8'9 lineage estimated by the Bayesian analysis are reported in Supplementary Data 28. Within the Italian mitochondrial variability, individual ST2 from Sicily, dated to 13,000 years BP, represents the most basal lineage of the Epigravettian-related specimens, including the older Tagliente 2 and Le Mura 1 samples. In this context, Le Mura 1 is phylogenetically closer to Paglicci 148, a Late Upper Palaeolithic specimen from Paglicci cave (Apulia), dated around 13,000 years BP (Supplementary Figure 12). The TMRCA of the U2'3'4'7'8'9 sequences in the Italian Epigravettian hunter-gatherers was estimated at 20,619 years BP (95% HPD: 17,817-23,743) (Supplementary Data 28).

The Y chromosome haplogroup was inferred using Yleaf v2.2 software [30]. Le Mura 1 belongs to the I2a lineage, sub-clade I2a1a1 (Supplementary Data 9). Haplogroup I2 has been identified in Tagliente 2 [23], ST5 [31] and in Upper Palaeolithic hunter-gatherers from Switzerland, Hungary and Scandinavia. Alongside R1a, I2 is the most frequent lineage found among male remains of the Villabruna cluster [32] and in Mesolithic Europe, until ~6,000 BCE, when the mass migration of Middle Eastern farmers carrying the Y haplogroup sequence G2a occurred [33].

Population genetic analysis. As previously reported, the genetic variation of the European Late Palaeolithic and Mesolithic hunter-gatherers is distributed along two main axes [23,28,34] (Fig. 4a and Supplementary Figure 6b): one axis describes the genetic distribution of the "Eastern hunter-gatherer" (EHG) populations who carry Mal'ta related ancestry and show affinity with the *Sidelkino* cluster. The second axis represents the genetic variation of the Late Upper Palaeolithic individuals associated with the Magdalenian cultural complex and Mesolithic specimens from Iberia and central Europe, which retain traces of genetic contributions from a population related to the 35 ka Aurignacian Goyet Q116-1 individual, as well as the derived Fournol-related ancestry. Individuals belonging to the "Western hunter-gatherer" (WHG) group (recently identified as *Oberkassel* cluster), which show affinity with the so called *Villabruna* cluster and are characterized by a genetic resemblance with present-day Near Eastern populations [32], are located at the vertex of these two axes.

Principal Component Analysis (PCA) shows that post-LGM individuals are grouped in two main cluster, WHG (or *Oberkassel*) and EHG (or *Sidelkino*), outside the extant Eurasian population variability, while El Mirón and GoyetQ2 individuals are positioned towards the centre of the PC space, as previously described.

The Multi-Dimensional Scaling (MDS) and PCA analyses show that Le Mura 1 falls within the variation of the WHG populations (Fig. 4a and Supplementary Figure 6) outside the modern Eurasian variability. Congruent with the pattern observed in MDS (Fig. 4a and Supplemenatary Figure S6b), Le Mura 1 seems to be positioned between the previously identified [34] Group 2 and Group 3 (Fig. 5a). The genetic affinity of Le Mura 1 with these samples is also confirmed by outgroup *f3*-statistics analysis in the form *f3*(Mura, *X*;

Mbuti.SDG), where *X* is a list of Palaeolithic and Mesolithic individuals (Supplementary Data 11; Supplementary Figure 7). To further investigate the genetic similarity between these groups and the Le Mura 1 specimen, we performed an *f4*-statistics analysis in the form *f4*(Group3, Group2; Mura, Mbuti.SDG) (Supplementary Data 14). The significantly positive *f4*-statistics (Uzzo_EM, AC16; Mura, Mbuti.SDG *f4*= 0.002971 *Z*= 3.664, Uzzo_EM, Italy Mesolithic.SG; Mura, Mbuti.SDG *f4*= 0.003229 *Z*= 4.812 and Italy OrienteC, Italy Mesolithic.SG; Mura, Mbuti.SDG *f4*= 0.002517 *Z*= 3.354) revealed that Le Mura 1 is genetically closer to the individuals from Uzzo cave dated to 10,000 years BP and to the individual from Grotta d'Oriente dated to 14,000 years BP (Fig. 4b).

The tool qpWave 1200 in ADMIXTOOLS 7.0.1 was used to test the null hypothesis of gene homogeneity between Le Mura 1 and the other Epigravettian and Mesolithic individuals from Italy. In all cases, a p-value greater than 5% indicates no reason to reject the null hypothesis (Supplementary Data 16). To confirm the qpWave results, we used the tool qpAdm 1201 in ADMIXTOOLS 7.0.1. The supported "one-way" model, in which *Villabruna* ancestry is the source population, demonstrated that Le Mura 1's genome cannot be the result of admixture events between two or more known ancestral populations(Supplementary Data 15).

The genetic relationships and geographic structure within the Italian Epigravettian and Mesolithic hunter-gatherers were explored in more detail using a neighbor joining (NJ) tree built with MEGA X [35], utilising the pairwise 1-*f3*-outgroup statistics matrix. The most basal lineage in the NJ tree (Fig. 5a) corresponded to the individual from Pradis, from which the older north-eastern Italian specimens branch out. Another branching separates the samples from north-western and central Italy from hunter-gatherers of southern Italy. In this context, Le Mura 1 branches from the more recent Arene Candide 16 sample and from the Mesolithic Continenza group, representing the basal lineage giving rise to the Sicilian individuals. To further investigate the genetic connections between Epigravettian individuals from glacial refugia in southern Italy and Magdalenians from Iberian refugia, we calculated an *f4*-statistics in the form *f4*(*X*, *Y*; *Z*, Mbuti.SDG), where *X* are Le Mura 1 or Epigravettian samples from western-central Italy and Sicily, *Y* are Epigravettians from northern Italy, and *Z* are El Mirón or GoyetQ2 used as proxies for Magdalenians from south-western and central-northern Europe, respectively (Supplementary Data 20).

To explore possible genetic continuity in southern Italy between the pre-LGM Gravettian groups and the Epigravettian-related population, we performed an *f4*-statistics in the form *f4*(Mura, *X*; *Y*, Mbuti.SDG), where *X* is either OrienteC (~14,000 years BP), Mesolithic samples from Grotta Continenza (~11,900 years BP), Tagliente 2 (~17,000 years BP), or Bichon (13,700 years BP), while *Y* are Italian Gravettian individuals listed in Supplementary Data 21. To avoid potential biases introduced by different genotyping strategies [34], we restricted the analysis to shotgun data. In order to investigate the genetic variability between Italian groups, we carried out the pairwise mismatch rate analysis (PMR) on genotype data in Eigenstrat format using a python script (https://github.com/TCLamnidis/pMMRCalculator) (Supplementary Data 18).

Dating of Neanderthal admixture. A late admixture with Neanderthals was detected, dating back 814 +/- 122.77 generations, which was estimated to have occurred 40,623 +/- 3,560 years BP. Since the method used should be reliable for samples with <35% missing data for established SNPs and for dates of admixture between 100-1,500 generations ago, the data obtained for Le Mura 1 can be considered accurate. Assuming a single gene flow event occurred approximately 814 generations earlier, as previously estimated, we inferred the age of the genome of Le Mura 1. The difference in the date of Neanderthal gene flow in the European extant and Le Mura 1 genomes translates into a direct estimate of the age of the ancient genome (Moorjani et al 2016). There is relatively close correspondence between the radiocarbon date of the sample (17,090–16,845 cal BP) and the age estimated using this approach (20,230 +/- 7,429) (Supplementary Data 22). To evaluate the robustness of the result, we repeated our analysis with genome wide data of Italian hunter-gatherers. For each sample, the estimate of the number of generations since the last Neanderthal admixture is reported in Supplementary Data 22. The high percentage of missing SNPs for the individuals genotyped with target enrichment strategy and the recent age of specimens from Continenza cave make these data unreliable.

Neanderthal and Denisova introgressed segments along the genome. We identified a total of 160.87 cM of archaic DNA (157.84 cM of Neanderthal origin and 3.03 cM of Denisova origin) (Supplementary Figure 11) with a mean fragment length of 0.061 cM and 0.014 cM for Neanderthal and Denisovan segments, respectively. Only one segment longer than 1 cM (1.02 cM) was detected on chromosome 18 (chr18: 59,694,981-60,718,327). Due to the short Neanderthal fragments recovered in the genome of Le Mura 1, we were not able to distinguish recent introgression events.

Moreover, we tested whether the called Neanderthal ancestry in the Le Mura 1 genome overlaps with known deserts of Neanderthal ancestry, which are large regions nearly devoid of any Neanderthal introgressed DNA [36]. Le Mura 1 carries almost no Neanderthal DNA in the deserts (1.21 cM out of 136.37 cM = 1.63 out of 133.14 MB).

Analysis of phenotypically informative markers. Two heterozygous mutations were identified in two different genes (TNNT2 and MYBPC3) linked to familial hypertrophic cardiomyopathy (FHC or HCM) (Supplementary Data 24), which – to our knowledge – had not been reported before in ancient individuals. HCM is a rare congenital heart defect characterized by ventricular thickening and it is a significant cause of sudden cardiac arrest and death in young adults and children [37,38]. HCM exhibits an autosomal dominant pattern of inheritance [39], with several genes implicated in this heart disorder [40–42]. The first variant identified (TNNT2: c.311G>A) was covered by 7 reads, one of which supported the alternate allele. This is quite a rare mutation, detected in only 6 patients [43], and the available evidence is currently insufficient to determine its role in the disease. However, the c.311G>A mutation is classified as "Pathogenic" in ClinVar. The second mutation, located in the MYBPC3 gene (c.529C>T, total depth of coverage=5, with only 1 read carrying the alternate allele), is classified as having "Conflicting interpretations of pathogenicity", although the most severely affected patients possess this variant in conjunction with mutations in other genes [40]. Usually, HCM patients carry one heterozygous mutation, but in 3-5% of cases two mutations are reported (in the same or in different genes), which are associated with a more severe phenotype and an earlier age of onset (often <10 years) [44,45]. Despite the low depth of coverage and the possibility of sequencing errors, these 2 SNPs appear highly reliable as they are positioned in the middle of the reads, with the highest genotype likelihood value inferred for both (loglikeratios to the most likely, scaled as log10, = 0). Furthermore, common practices to avoid errors due to post-mortem damage, such as the usage of half-UDG libraries and a 4-base trimming performed at both ends of the reads, support the authenticity of these heterozygous mutations.

Several additional functional and phenotypic traits can be inferred from the genome data (Supplementary Data 24). Three variants (rs12203592 on the IRF4 gene, rs1042602 on the TYR gene, and rs4778138 on the OCA2 gene) suggest possible phenotypes for freckles. A CC genotype SNP (reverse strand) on ABCC11 gene on chromosome 16 is consistent with the Le Mura 1 individual having wet earwax type and normal body odour. Additionally, five different SNPs suggest that Le Mura 1 probably had a normal/slightly higher body mass index. By screening a number of SNPs associated with ABO blood group polymorphisms, we predicted that Le Mura 1 could have been type O. All functional SNPs annotated are listed in Supplementary Data 24.

Supplementary References

1. De Michele, E. Grotta delle Mura - Monopoli (Bari) V - Speleologenesi in relazione al carsismo locale. in *Atti della Socieetà Italiana di Scienze Naturali e del Museo Civico di Storia Naturale di Milano* 3–29 (Milano, 1965).

2. Calattini, M. Scoperta di una sepoltura paleolitica a Grotta delle Mura (BA). *Rassegna di archeologia : preistorica e protostorica* 37–45 (2002) doi:10.1400/248076.

3. Calattini, M. Il livello dell'Epigravettiano finale di Grotta delle Mura (Bari) : area A. *Il livello dell'Epigravettiano finale di Grotta delle Mura (Bari) : area A.* 305–320 (2005) doi:10.1400/206818.

4. Reimer, P. J. *et al.* The IntCal20 Northern Hemisphere Radiocarbon Age Calibration Curve (0-55 cal kBP). *Radiocarbon* **62**, 725–757 (2020).

5. Bronk Ramsey, C. Bayesian analysis of radiocarbon dates. *Radiocarbon* **51**, 337–360 (2009).

6. Calattini, M. *et al.* Il bambino dell'Epigravettiano Finale rinvenuto nella Grotta delle Mura a Monopoli (Bari). in *Atti XV Congresso dell'Associzione Antropologica Italiana* (eds. Michetti, E., Di Fabrizio, A., D'Anastasio, R. & Capasso, L.) 125–134 (Chieti, 2003).

7. Calattini, M. Il livello Epigravettiano (US 130) di grotta delle Mura (Bari). in *Atti 21 Convegno Nazionale sulla Preistoria e Protostoria della Daunia* 3–12 (San Severo, 2001).

8. Berto, C., Boscato, P., Boschin, F., Luzi, E. & Ronchitelli, A. Paleoenvironmental and paleoclimatic context during the Upper Palaeolithic (late Upper Pleistocene) in the Italian Peninsula. The small mammal record from Grotta Paglicci (Rignano Garganico, Foggia, Southern Italy). *Quat Sci Rev* **168**, 30–41 (2017).

9. Bon, M. & Boscato, P. Associazioni faunistiche dell'Olocene antico nell'Italia del sud: confronto tra un sito adriatico (Grotta delle Mura, Monopoli, Bari) ed uno tirrenico (Grotta della Serratura, Marina di Camerota, Salerno). *Italian Journal of Quaternary Science* **9**, 567–572 (1996).

10. Stloukal, M. & Hanakova, H. Die Longe der langskonochen altslavischer Bevolkerungen unter besonderer Bercksichtigung von Wachstumsfragen. *Homo* **29**, 53–69 (1978).

11. Moorrees, C. F. A., Fanning, E. A. & Hunt, E. E. Formation and resorption of three deciduous teeth in children. *Am J Phys Anthropol* **21**, 205–213 (1963).

12. Moorrees, C. F. A., Fanning, E. A. & Hunt, E. E. Age variation of formation stages for ten permanent teeth. *J Dent Res* **42**, 1490–1502 (1963).

13. AlQahtani, S. J., Hector, M. P. & Liversidge, H. M. Brief communication: The London atlas of human tooth development and eruption. *Am J Phys Anthropol* **142**, 481–490 (2010).

14. Boccone, S., Micheletti Cremasco, M., Bortoluzzi, S., Moggi-Cecchi, J. & Rabino Massa, E. Age estimation in subadult Egyptian remains. *HOMO- Journal of Comparative Human Biology* **61**, 337–358 (2010).

15. Cunningham, C., Scheuer, L. & Black, S. *Developmental Juvenile Osteology*. *Developmental Juvenile Osteology (Second Edition)* (Academic Press, 2017).

16. Murphy, T. Gradients of dentine exposure in human molar tooth attrition. *Am J Phys Anthropol* **17**, 179–186 (1959).

17. Molnar, S. Human tooth wear, tooth function and cultural variability. *Am J Phys Anthropol* **34**, 175–189 (1971).

18. Romanelli, M. C. *et al.* Diagnosi differenziale fra lesioni da parto e child abuse: considerazioni medico-legali a margine di un caso peritale. *Zacchia* **XXX-Serie 4a**, 1–4 (2016).

19. Floyd, R. C. & Smeltzer, J. S. Shoulder dystocia. in *Clinical Maternal-Fetal Medicine Online* 13.1-13.9 (CRC Press, London, 2021). doi:10.1201/9781003222590-11.

20. Weissensteiner, H. *et al.* HaploGrep 2: mitochondrial haplogroup classification in the era of high-throughput sequencing. *Nucleic Acids Res* **44**, W58–W63 (2016).

21. van Oven, M. PhyloTree Build 17: Growing the human mitochondrial DNA tree. *Forensic Sci Int Genet Suppl Ser* **5**, (2015).

22. Posth, C. *et al.* Pleistocene mitochondrial genomes suggest a single major dispersal of non-africans and a late glacial population turnover in Europe. *Current Biology* **26**, (2016).

23. Bortolini, E. *et al.* Early Alpine occupation backdates westward human migration in Late Glacial Europe. *Current Biology* **31**, 2484-2493.e7 (2021).

24. Yu, H. *et al.* Genomic and dietary discontinuities during the Mesolithic and Neolithic in Sicily. *iScience* **25**, (2022).

25. Modi, A. *et al.* More data on ancient human mitogenome variability in Italy: new mitochondrial genome sequences from three Upper Palaeolithic burials. *Ann Hum Biol* **48**, 213–222 (2021).

26. Modi, A. *et al.* Paleogenetic and morphometric analysis of a Mesolithic individual from Grotta d'Oriente: An oldest genetic legacy for the first modern humans in Sicily. *Quat Sci Rev* **248**, 106603 (2020).

27. Catalano, G. *et al.* A mitogenome sequence of an Equus hydruntinus specimen from Late Quaternary site of San Teodoro Cave (Sicily, Italy). *Quat Sci Rev* **236**, 106280 (2020).

28. Villalba-Mouco, V. *et al.* Survival of Late Pleistocene Hunter-Gatherer Ancestry in the Iberian Peninsula. *Current Biology* **29**, 1169-1177.e7 (2019).

29. Behar, D. M. *et al.* A 'copernican' reassessment of the human mitochondrial DNA tree from its root. *Am J Hum Genet* **90**, 675–684 (2012).

30. Ralf, A., Montiel González, D., Zhong, K. & Kayser, M. Yleaf: Software for Human Y-Chromosomal Haplogroup Inference from Next-Generation Sequencing Data. *Mol Biol Evol* **35**, 1291–1294 (2018).

31. Scorrano, G. *et al.* Bioarchaeological and palaeogenomic portrait of two Pompeians that died during the eruption of Vesuvius in 79 AD. *Sci Rep* **12**, 1–12 (2022).

32. Fu, Q. *et al.* The genetic history of Ice Age Europe. *Nature* **534**, 200–205 (2016).

33. Kivisild, T. The study of human Y chromosome variation through ancient DNA. *Human Genetics* vol. 136 Preprint at https://doi.org/10.1007/s00439-017-1773-z (2017).

34. Posth, C. *et al.* Palaeogenomics of Upper Palaeolithic to Neolithic European hunter-gatherers. *Nature* **615**, 117–126 (2023).

35. Kumar, S., Stecher, G., Li, M., Knyaz, C. & Tamura, K. MEGA X: Molecular evolutionary genetics analysis across computing platforms. *Mol Biol Evol* **35**, 1547–1549 (2018).

36. Vernot, B. *et al.* Excavating Neandertal and Denisovan DNA from the genomes of Melanesian individuals. *Science (1979)* **352**, (2016).

37. Bagnall, R. D. *et al.* A Prospective Study of Sudden Cardiac Death among Children and Young Adults. *New England Journal of Medicine* **374**, 2441–2452 (2016).

38. Autore, C. & Musumeci, M. B. The natural history of hypertrophic cardiomyopathy. *Eur Heart J Suppl* **22**, L11–L14 (2020).

39. Greaves, S. C., Roche, A. H. G., Neutze, J. M., Whitlock, R. M. L. & Veale, A. M. O. Inheritance of hypertrophic cardiomyopathy: A cross sectional and M mode echocardiographic study of 50 families. *Heart* **58**, (1987).

40. Wells, Q. S. *et al.* Familial Dilated Cardiomyopathy Associated with Congenital Defects in the Setting of a Novel VCL Mutation (Lys815Arg) in Conjunction with a Known MYPBC3 Variant. *Cardiogenetics* **1**, (2011).

41. Alfares, A. A. *et al.* Results of clinical genetic testing of 2,912 probands with hypertrophic cardiomyopathy: Expanded panels offer limited additional sensitivity. *Genetics in Medicine* **17**, (2015).

42. Marian, A. J. & Braunwald, E. Hypertrophic cardiomyopathy: Genetics, pathogenesis, clinical manifestations, diagnosis, and therapy. *Circ Res* **121**, (2017).

43. Pan, S., Caleshu, C. A., Dunn, K. E. & Ashley, E. A. Cardiac structural and sarcomere genes associated with cardiomyopathy exhibit marked intolerance of genetic variation. *Circ Cardiovasc Genet* **5**, 602–610 (2012).

44. Richard, P. *et al.* Hypertrophic Cardiomyopathy. *Circulation* **107**, 2227–2232 (2003).

45. Christiaans, I. *et al.* Founder mutations in hypertrophic cardiomyopathy patients in the Netherlands. *Netherlands Heart Journal* **18**, 254 (2010).